AAAS
Journal of Remote Sensing
Volume 2021, Article ID 9842702, 13 pages
https://doi.org/10.34133/2021/9842702

Journal of Remote Sensing
A SCIENCE PARTNER JOURNAL

Research Article

Impact of Temperature on Absorption Coefficient of Pure Seawater in the Blue Wavelengths Inferred from Satellite and *In Situ* Measurements

Guomei Wei,[1,2] Zhongping Lee,[3] Xiuling Wu,[1] Xiaolong Yu,[1] Shaoling Shang,[1] and Ricardo Letelier[4]

[1]*State Key Laboratory of Marine Environmental Science, College of Ocean and Earth Sciences, Xiamen University, Xiamen 361102, China*
[2]*Research and Development Center for Ocean Observation Technologies, Xiamen University, Xiamen 361102, China*
[3]*School for the Environment, University of Massachusetts Boston, Boston, MA 02125, USA*
[4]*College of Earth, Ocean & Atmospheric Sciences, Oregon State University, Corvallis, OR 97331, USA*

Correspondence should be addressed to Zhongping Lee; zhongping.lee@umb.edu

Received 12 March 2021; Accepted 16 June 2021; Published 13 July 2021

There has been a long history of interest on how (if) the absorption coefficient of "pure" fresh water ($a_{fw}(\lambda)$) and "pure" seawater ($a_{sw}(\lambda)$) changes with temperature (T), yet the impact of T reported in the literature differs significantly in the blue domain. Unlike the previous studies based on laboratory measurements, we took an approach based on ~18 years (2002–2020) of MODIS ocean color and temperature measurements in the oligotrophic oceans, along with field measured chlorophyll concentration and phytoplankton absorption coefficient, to examine the relationship between T and the total absorption coefficient ($a(\lambda)$) at 412 and 443 nm. We found that the values of $a(412)$ and $a(443)$ in the summer are nearly flat (slightly decreasing) for the observed T range of ~19–27 °C. Since there are no detectable changes of chlorophyll during this period, the results suggest that T has a negligible impact on $a_{sw}(412)$ and $a_{sw}(443)$ in this T range. As a complement, the impact of salinity on $a_{fw}(\lambda)$ was also evaluated using three independent determinations of $a_{sw}(\lambda)$ and $a_{fw}(\lambda)$, where good agreements were found from these observations.

1. Introduction

The absorption coefficient of "pure" fresh water ($a_{fw}(\lambda)$, in m^{-1}) and "pure" seawater ($a_{sw}(\lambda)$) is a basic inherent optical property (IOP) [1]; together with the incident radiation spectrum, scattering, and the optical characteristics of other constituents, they determine the apparent color of water [2]. It is thus a fundamental requirement to know the values of $a_{fw}(\lambda)$ and $a_{sw}(\lambda)$ and how (or if) they change with environmental conditions, such as temperature and salinity. To meet this desire, there is a long history in estimating $a_{fw}(\lambda)$ and $a_{sw}(\lambda)$ (Fewell and von Trojan [3], and references therein), with $a_{fw}(\lambda)$ values in the ~370–700 nm determined by Pope and Fry [4] in laboratory measurements adopted as the "standard" by the ocean color community in the past two decades. Recently, Mason et al. [5] updated $a_{fw}(\lambda)$ using an improved integrating cavity and found that $a_{fw}(\lambda)$ values are significantly lower (by a factor of up to 5, see Figure 11 in Mason et al. [5]) than those reported in Pope and Fry [4] for wavelengths ranging from 250 to 500 nm. In addition, the values in the UV-blue domain (350–420 nm) of Mason et al. [5] are significantly lower than those reported in Lee et al. [6], with the latter considered to represent the absorption coefficient of "pure" seawater.

Further, since there are strong variations of temperature (T, in °C) in the aquatic environment, there has been a long history of interest in how (if) $a_{fw}(\lambda)$ and $a_{sw}(\lambda)$ change with T, with the first reported estimation made by Wild in 1868 (cited in Trabjerg and Hojerslev [7]). In the recent decades, and with modern instrumentation, Trabjerg and Hojerslev [7] found that $a_{fw}(\lambda)$ and $a_{sw}(\lambda)$ decrease with T. In contrast, Pegau et al. [8] obtained an increase effect of T on $a_{sw}(\lambda)$, while recently both Sullivan et al. [9] and Röttgers et al. [10] indicated that T has a negligible impact on $a_{fw}(\lambda)$. Note

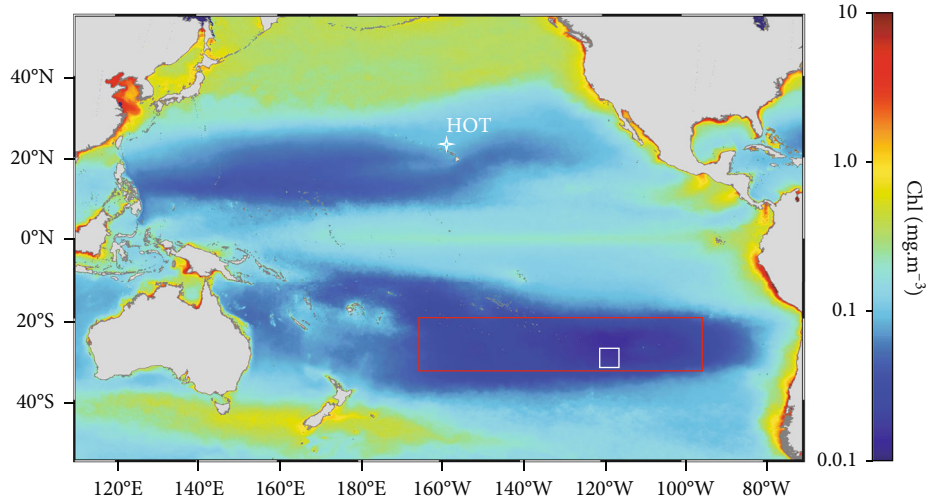

Figure 1: Location of data used in this study. The Hawaii Ocean Time-series (HOT; white star symbol), center of the South Pacific Gyre (cSPG, the white box), and the entire SPG (the red box). The background image is the Chl climatology in winter (December to February) obtained from MODIS-Aqua (downloaded from the NASA OBPG).

that all these reports were based on laboratory measurements with prepared "pure" water or artificial seawater and using tubes or integrating spheres with path lengths 25 cm to ~100 cm. Because $a_{fw}(\lambda)$ and $a_{sw}(\lambda)$ values in the UV-blue domain are very low [5], change of light intensity passing through such a short tube is in the order of ~10^{-4}–10^{-3}, which places a significant demand on the sensitivity and calibration of the sensors and systems [10], in addition to the preparation of "pure" fresh water or "pure" seawater. Such extremely small changes in light intensity, as well as the challenge to calibrate the measurement system under different temperature, might be the main reasons for the discrepancies on the relationship between a_{fw} or $a_{sw}(\lambda)$ and T. As indicated in Sullivan et al. [9], the uncertainty of such measurements is around 0.001 m^{-1}, corresponding to approximately 45% of the $a_{fw}(400)$ value reported in Mason et al. [5].

In this study, rather than estimating $a_{sw}(\lambda)$ in a laboratory setting, we took an approach of analyzing the relationship between T and the total absorption coefficient (a) at 412 nm and 443 nm obtained from ~18 years of ocean color satellites and combining field measurements of chlorophyll concentration (Chl, in mg m^{-3}), phytoplankton absorption coefficient (a_{ph}, in m^{-1}), and sea surface temperature (represented as T in this article). Specifically, for T in local summer months varying between ~19 and 27 °C and stable Chl concentration, we calculated the regression slope between a(412) and a(443) and T and found that they are not different than 0 (slight negative), contrasting with the results about $a_{sw}(\lambda)$ reported in Trabjerg and Hojerslev [7] and Pegau et al. [8]. The results are rather similar to those of Sullivan et al. [9] and Röttgers et al. [10], although they obtained the dependence of $a_{fw}(\lambda)$. We selected these two wavelengths in our analysis because (1) they are the shortest blue wavelengths for MODIS (the Moderate Resolution Imaging Spectroradiometer) and (2) they display the strongest dependence of $a_{sw}(\lambda)$ on T [7, 8] among the MODIS channels. Note that it is unclear if the temperature effect is the same on $a_{fw}(\lambda)$ and $a_{sw}(\lambda)$, so comparisons and discussions are focused on the T effect of $a_{sw}(\lambda)$ as $a(\lambda)$ from MODIS is for natural oceanic waters.

2. Data

2.1. HOT Time Series. Data from the ongoing Hawaii Ocean Time-series program (HOT, https://hahana.soest.hawaii.edu/hot/) were employed to validate the temporal patterns of Chl and a_{ph} obtained from MODIS. Station ALOHA, sampled by the HOT program at nearly monthly intervals since 1988, is located at 22° 45′ N, 158° 00′ W in the North Pacific Gyre (the white star symbol in Figure 1) and was established to provide systematic and repeated observations of the hydrography, chemistry, and biology of the water column. The data used in this study cover 81 pairs of Chl (by fluorometric method) and T for water at 2.5–5 m from the sea surface. In addition, a_{ph} at 5 m and 25 m were used to represent surface values of the phytoplankton absorption coefficient. Details of the cruises and measurement methods can be found in Letelier et al. [11].

2.2. MODIS Time Series. MODIS-Aqua globally mapped 8-day composite of remote-sensing reflectance ($R_{rs}(\lambda)$, in sr^{-1}) with a 4 km resolution, for the period of July 2002 to July 2020, processed with the most recent updates in calibration and algorithms (2018 reprocessed version), was obtained from the NASA Ocean Biology Processing Group (OBPG, http://oceancolor.gsfc.nasa.gov/). The center wavelengths of these $R_{rs}(\lambda)$ are 412, 443, 488, 547, and 667 nm. The concurrent MODIS-Aqua globally mapped 8-day composite of T product (2019 reprocessed version) with the same resolution was also downloaded from the OBPG website. Further, data from three areas are utilized for this effort, which are HOT, center of the South Pacific Gyre (SPG), and the entire SPG.

2.2.1. HOT. In order to obtain a statistically significant number of points having concurrent MODIS ocean color and T measurements, the data within a 10 km distance of HOT are extracted from the downloaded global MODIS data. To minimize the impact of random spikes resulting from satellite measurements and processing, for each 8 days and each band, the $R_{rs}(\lambda)$ mode value was calculated based on all of the $R_{rs}(\lambda)$ values within the 10 km distance of HOT. This mode $R_{rs}(\lambda)$ value was then used to represent the property of HOT for that band. The same processing scheme was applied to obtain the T data, and a time series (with a temporal resolution of 8 days) over 18 years for both $R_{rs}(\lambda)$ and T was assembled.

2.2.2. Center of the South Pacific Gyre. Similarly as HOT, the data from the "center" of the South Pacific Gyre (cSPG), which is defined as 27–32° S, 115–120° W (the white box in Figure 1) was employed to evaluate the relationships between $a(412, 443)$ and T. This region is located within the zone of the "clearest" natural waters [12], where $a_{sw}(\lambda)$ play the largest role at the blue wavelengths (can account for up to ~50% of $a(412)$) compared to other natural waters. For this small box, the mode $R_{rs}(\lambda)$ and T are produced following the same procedure described above.

2.2.3. Entire South Pacific Gyre. To avoid any coincidental observations that might be specific to cSPG, we expanded the analysis to the entire SPG (the red box in Figure 1) in order to further examine the impact of T on $a_{sw}(\lambda)$. To emphasize the contribution from $a_{sw}(\lambda)$, the analyses are limited to pixels where Chl is always less than 0.07 mg m^{-3} in the 18-year time series (i.e., from July 2002 to July 2020), where 0.07 mg m^{-3} is considered as a criterion for classifying oceanic gyre waters [13, 14]. At the same time, we found that T has a seasonal variation of ~10 °C, sufficient to cause detectable change in $a_{sw}(412)$ and $a_{sw}(443)$ if the previously reported temperature dependence of a_{sw} by Trabjerg and Hojerslev [7] and Pegau et al. [8] is real.

For this larger area, the quality control of $R_{rs}(\lambda)$ and T at each pixel (4 km data) is based on the following criteria: $R_{rs}(\lambda)$ at the five bands (412, 443, 488, 547, and 667 nm) are positive and <0.05 sr^{-1} and the T value having qual_sst (quality flag of sea surface temperature) ≤ 2, i.e., the bad and not processed T values were removed. Further, each pixel in this box is treated independently, i.e., no further spatial averaging.

3. Method to Obtain the Total Absorption Coefficient

3.1. Inversion of $a(\lambda)$ from $R_{rs}(\lambda)$. Ideally, we should use field measured $a_{sw}(\lambda)$ or $a(\lambda)$ to analyze the impact of T. However, there are no such long-term data obtained in the oligotrophic ocean, and there are various levels of uncertainties from *in situ* measurements [15, 16]; we thus used the long-term, high-quality MODIS $R_{rs}(\lambda)$ in the oligotrophic ocean to fill this void. Because the diffuse attenuation coefficient in the short blue wavelengths is around 0.02 m^{-1} for such oligotrophic waters [12, 17], the penetration depth [18] can be as deep as ~50 m for such waters. Thus, $a(412)$ and $a(443)$ can be considered measured equivalently with a "tube" as long as 50 m, greatly longer than the path length taken in lab measurement settings. As a result, the sensitivity of the absorption coefficient measurement is substantially improved.

There are many semianalytical algorithms developed in the past decades for the inversion of $a(\lambda)$ from $R_{rs}(\lambda)$ [19], where most of them require biooptical models for the component absorption coefficients (e.g., a_{ph}) and to specify $a_{sw}(\lambda)$ in the process, thus preventing an independent analysis regarding the impact of T on $a_{sw}(\lambda)$. The quasi-analytical algorithm (QAA) developed by Lee et al. [20] (the latest update version 6, http://www.ioccg.org/groups/Software_OCA/QAA_v6_2014209.pdf), as described below, is used in this effort for two reasons. First, QAA does not need to model the component absorption coefficient in the inversion process, and second, it needs only the $a_{sw}(\lambda)$ value at one wavelength (547 nm in the present analysis). Therefore, QAA offers a feasible means to analyze the T effect on $a_{sw}(\lambda)$ in the shorter wavelengths. A brief description of QAA is provided below to highlight the concept and the key components.

Earlier studies [2, 21] have shown that $R_{rs}(\lambda)$ can be expressed as

$$R_{rs} = G\frac{b_b}{a + b_b}, \tag{1}$$

where G (sr^{-1}) is a model parameter. For each R_{rs}, there are two unknowns: a and the total backscattering coefficient (b_b, in m^{-1}); thus, knowing a enables the calculation of b_b or vice versa.

For oligotrophic waters and $R_{rs}(\lambda)$ obtained from MODIS, $a(547)$ can be approximated as $a_{sw}(547)$; hence, $b_b(547)$ can be calculated algebraically from known $R_{rs}(547)$ and $a(547)$. Further, the particle backscattering coefficient at 547 nm ($b_{bp}(547)$) is obtained from $b_b(547)$ after subtracting $b_{bw}(547)$ (the backscattering coefficient of pure seawater). The $b_{bp}(547)$ is extended to the shorter wavelengths based on the power-law model of the particle backscattering coefficient [2].

$$b_{bp}(\lambda) = b_{bp}(547)\left(\frac{547}{\lambda}\right)^{Y}, \tag{2}$$

with Y estimated empirically from [20]

$$Y = 2.0\left(1 - 1.2\ \exp\left(-0.9\frac{R_{rs}(443)}{R_{rs}(547)}\right)\right). \tag{3}$$

For oligotrophic waters, as $R_{rs}(443)/R_{rs}(547) > 5$, the Y value estimated by Equation (3) is effectively ~2.0. Further, $a(\lambda)$ at 412 and 443 nm are calculated algebraically from $R_{rs}(\lambda)$ after $b_{bp}(\lambda)$ are derived following Equations (2)–(3) and $b_{bw}(\lambda)$ from Zhang et al. [22], with the results corresponding to $a(412)_{QAA}$ and $a(443)_{QAA}$.

It is required to know the value of $a_{sw}(547)$ for the above derivations, which we adopt from Pope and Fry [4] and

consider invariant for changing temperature and salinity [9, 10]. In addition, it is required to know the backscattering coefficient of pure seawater ($b_{bsw}(\lambda)$), with values from Zhang et al. [22] used here. Note that for T in a range of ~15–30 °C and salinity in a range of ~33–34 PSU, the variation of $b_{bsw}(\lambda)$ is within ~0.8%, which is negligible in the present study.

3.2. Estimation of Chl from $R_{rs}(\lambda)$. As this study focuses on extremely oligotrophic waters, the band-difference algorithm in Hu et al. [23], which is more robust than the traditional band-ratio scheme for such waters, is employed for the estimation of Chl from ocean color. Specifically, a color index (CI) is defined as

$$\mathrm{CI} = R_{rs}(555) - \left[R_{rs}(443) + \frac{555-443}{667-443}\left(R_{rs}(667) - R_{rs}(443)\right)\right]. \quad (4)$$

Because the MODIS green band is centered at 547 nm instead of 555 nm for SeaWiFS, MODIS $R_{rs}(547)$ was converted to $R_{rs}(555)$ by multiplying 0.93 [23]. Further, Chl is estimated from CI,

$$\mathrm{Chl} = 10^{-0.4909+191.6590*\mathrm{CI}}, \quad \left(\mathrm{CI} \leq -0.0005\ \mathrm{sr}^{-1}\right). \quad (5)$$

3.3. Modeling $a(\lambda)$ Based on Chl and T. The QAA shows a direct scheme to obtain $a(\lambda)$ from $R_{rs}(\lambda)$. Another scheme, which is indirect and based on Chl, can also be utilized to obtain $a(\lambda)$ from $R_{rs}(\lambda)$. The core assumption for this scheme is the "Case 1" concept where the variation in optical properties of such waters can be expressed using Chl [24–28]. Specifically, $a(\lambda)$ can be expressed as

$$a(\lambda, T)_{\mathrm{Chl}} = a_{sw}(\lambda, T) + a_{ph}(\lambda) + a_{dg}(\lambda) = a_{sw}(\lambda, T) + a_{pg}(\lambda), \quad (6)$$

where $a_{dg}(\lambda)$ is the combined absorption by detrital particulate matter and gelbstoff and $a_{pg}(\lambda) = a_{ph}(\lambda) + a_{dg}(\lambda)$. Further, $a_{ph}(\lambda)$ and $a_{dg}(\lambda)$ can be modeled as

$$a_{ph}(\lambda) = a^{*}_{ph}(\lambda)\mathrm{Chl}, \quad (7)$$

$$a_{dg}(\lambda) = a_{dg}(443)e^{-S_{dg}(\lambda-443)}. \quad (8)$$

$a^{*}_{ph}(\lambda)$ is the "Chl-specific" absorption coefficient, which can be modeled as a function of Chl [24, 25].

$$a^{*}_{ph}(\lambda) = A(\lambda)\mathrm{Chl}^{-\mathrm{B}(\lambda)}, \quad (9)$$

with the wavelength-dependent$A(\lambda)$ and $B(\lambda)$parameters obtained from extensive measurements in oceanic waters [24]. For oceanic "Case 1" waters, $a_{dg}(443)$ covary with Chl [25, 29]; then, a relationship between $a_{dg}(443)$ and $a_{ph}(443)$ is set as

$$a_{dg}(443) = p\, a_{ph}(443). \quad (10)$$

A p value of 1.0 is used here [30]. S_{dg} is the spectral slope for the gelbstoff absorption coefficient, and in this study, it is set as 0.014 nm^{-1} following Bricaud et al. [31].

Thus, for the given $R_{rs}(\lambda)$ and T, the total absorption coefficient (represented as $a(\lambda, T)_{\mathrm{Chl}}$) of such "Case 1" waters could also be calculated after values of $a_{sw}(\lambda, T)$ are provided, where the variation of $a_{sw}(\lambda)$ due to T could be characterized. Since the most recent temperature dependence of a_{sw} was reported by Trabjerg and Hojerslev [7] and Pegau et al. [8], only their temperature relationships, respectively, were included in the comparisons. It is necessary to point out that, although there are various levels of uncertainties in the R_{rs} to Chl and Chl to $a(\lambda)_{\mathrm{Chl}}$, the role of Chl in this scheme for the total absorption coefficient is rather a "middleman." Fundamentally, it is an empirical system that allows us to estimate $a(\lambda)$ from R_{rs}. In the empirical relationships developed between R_{rs} and Chl as well as between Chl and $a_{ph}(\lambda)$, the impact of T average is included, implicitly, in the empirical coefficients.

4. Results

4.1. Temporal Patterns of Chl in Local Summer. The temporal patterns of Chl at both HOT and cSPG obtained from MODIS are presented in Figure 2, along with Chl of HOT measured fluorometrically. The MODIS Chl is in a range of 0.04–0.16 $\mathrm{mg\,m^{-3}}$ at HOT, which is generally consistent with *in situ* Chl (0.03–0.18 $\mathrm{mg\,m^{-3}}$) during 2002–2019. Further, as would be expected, Chl decreased generally from March to May at HOT and from September to November at cSPG in response to nutrient supply and photoadaptation to higher light levels, a result of increased mean daily photon flux in the mixed layer, i.e., increased stratification and day length [11, 13, 32, 33].

More importantly, for the summer months (July–September for HOT) where T varied in a range of 24.7–28.6 °C at HOT, we observe that Chl concentrations derived from both MODIS and *in situ* are quite stable and consistent (see Figure 2(c)), which is in agreement with that presented in Winn et al. [33]. The slope in linear regression between Chl and T during these months is 0.0010 $\mathrm{mg\,m^{-3}\,°C^{-1}}$ for MODIS Chl and 0.0008 $\mathrm{mg\,m^{-3}\,°C^{-1}}$ for *in situ* Chl, and there is no significant difference between these slopes. These comparisons and evaluations suggest that the temporal patterns of MODIS Chl for such oligotrophic waters for the summer months are reasonable. In addition, in viewing an average Chl of 0.06 $\mathrm{mg\,m^{-3}}$, the slope suggests negligible variation of Chl in the summer months (~7% change of Chl).

Comparisons between MODIS Chl and T at cSPG in December–February (austral summer) are shown in Figure 2(d). For T in a range of 19.6–27.0 °C, the slope between Chl and T is nearly flat (1×10^{-5} $\mathrm{mg\,m^{-3}\,°C^{-1}}$), which also indicates that Chl remains constant in the summer months though T varies by ~7.4 °C.

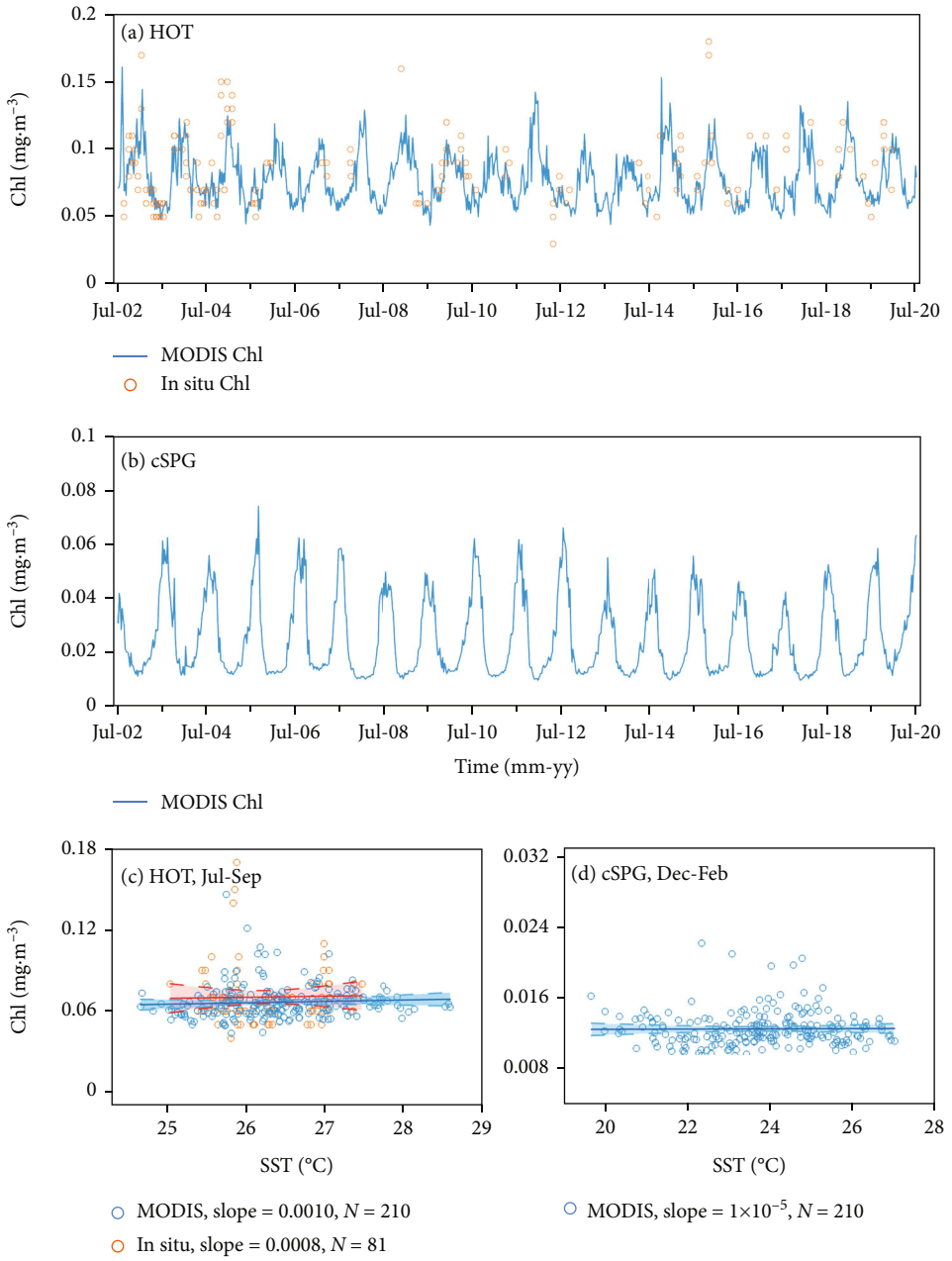

Figure 2: Time series of Chl at HOT (a) and cSPG (b) and relationships (c, d) between Chl and T during the local summer months (July–September for HOT, December–February for cSPG). Also included in (c) and (d) are the linear best fit (solid line) and 95% confidence interval (dash line) to each group of data along with its slope.

4.2. Characteristics of $a(412)_{QAA}$, $a(443)_{QAA}$, and T Time Series at cSPG. Because of seasonal variations in solar radiation and ocean dynamics, there are clear seasonal patterns (8-day resolution) in T and $a(412)_{QAA}$ and $a(443)_{QAA}$ for waters at cSPG, as presented in Figure 3. The $a(412)_{QAA}$ and $a(443)_{QAA}$ are in a range of ~0.009–0.02 m^{-1} and~0.01–0.02 m^{-1}, respectively, which are consistent with those reported in Bricaud et al. [31]. The T value is in a range of 17.7–27.0 °C with the difference between the climatological maximum summer and winter minimum values as ~9 °C.

There is a general, opposite relationship between the absorption coefficient and T (see Figure 4), with R^2 as 0.58 for 412 nm and 0.48 for 443 nm, respectively. The decrease of absorption with the increase of T is in general due to the decrease of Chl, a result of photoadaptation and stratification in the surface layer [11, 13, 33]. While the detailed temporal variations are important for the study of phytoplankton dynamics in the open ocean [13, 34], they are out of the scope of this study, and we will focus on the relationship between $a(\lambda)$ and T in the following. In particular, as indicated in Figures 3(c) and 4, although

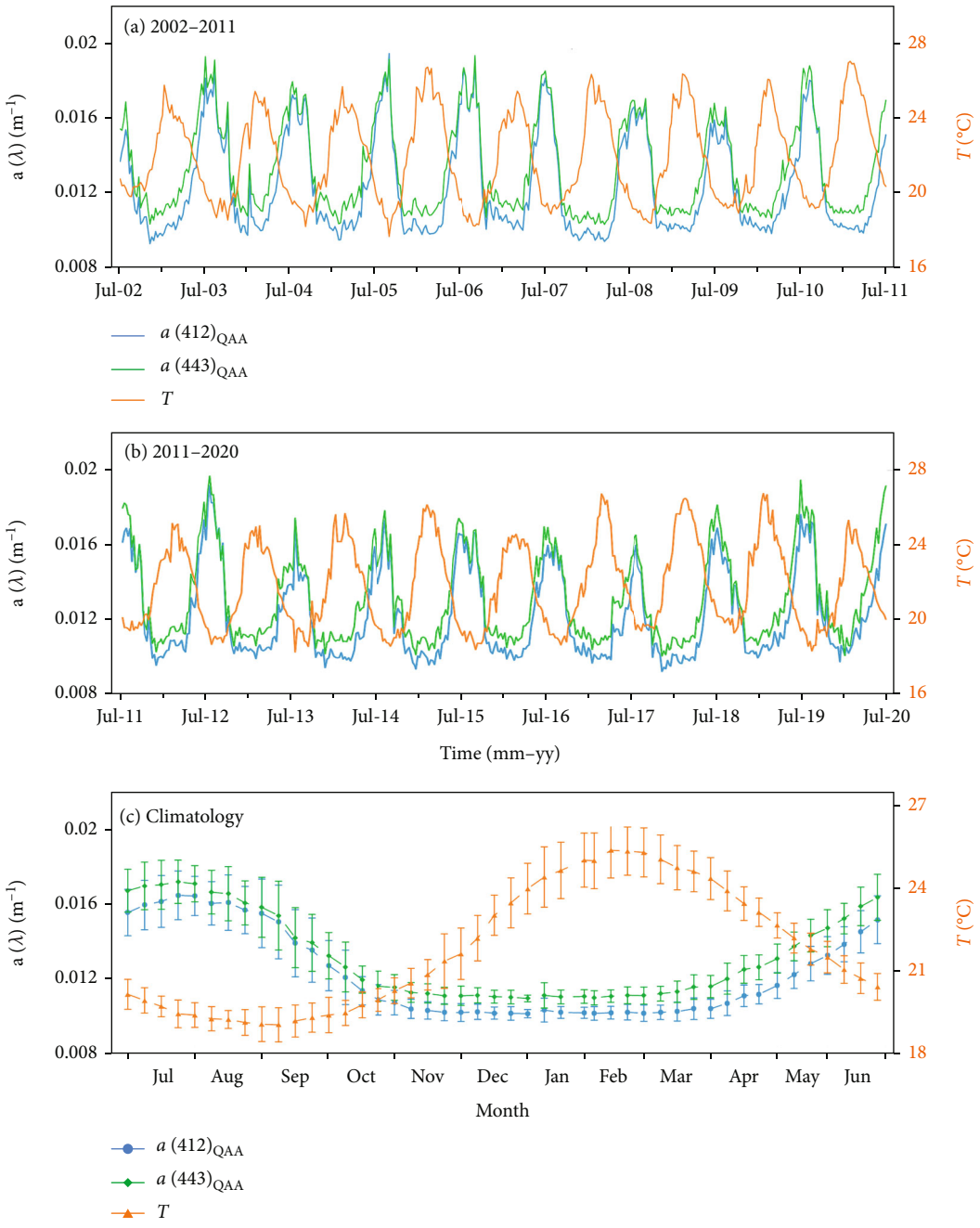

FIGURE 3: The 8-day time series of $a(412)_{QAA}$ (blue), $a(443)_{QAA}$ (green), and T (orange) for waters of cSPG during the period of July 2002 to July 2020: (a) for 2002-2011, (b) for 2011-2020, and (c) for 8-day climatology.

T varies a lot in the summer months, values of $a(\lambda)$ in this period are generally stable.

Following the approach used to analyze the temperature patterns of Chl in local summer, a trend of $a(\lambda)$ versus T in December–February (southern summer) can be drawn and shown in Figure 5. It is found that for T in a range of 19.6–27 °C, the slope between $a(412)_{QAA}$ and $a(443)_{QAA}$ and T is also nearly flat (slightly negative, -4×10^{-5} m^{-1}°C^{-1}), i.e., there are no obvious increases or decreases of the total absorption coefficient for T increased by ~7.4 °C. For comparison, these slopes, along with the T-dependent slopes of a_{sw} reported in previous studies, are listed in Table 1. Note that, as indicated by Figure 2(d), there are no changes of Chl for these summer months; thus, by Equation (6), a_{pg} are also expected to be stable; therefore, there should be a significant decrease (following Trabjerg and Hojerslev [7]) or an obvious increase (following Pegau et al. [8]) trend of $a(412)$ and $a(443)$ for the increase of T, as presented in Figure 5. In particular, the decrease of $a(412)$ is expected to be ~56% following Trabjerg and Hojerslev

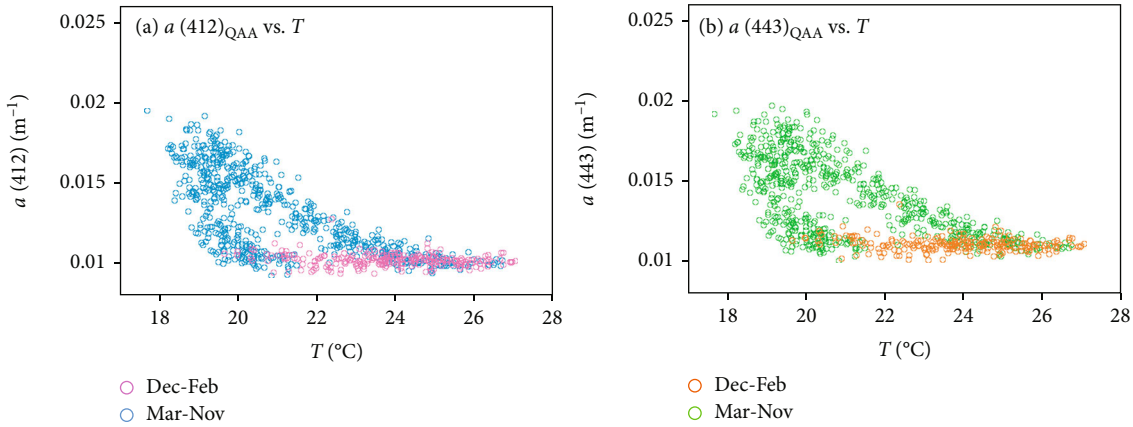

Figure 4: Relationships between T and $a(412)_{QAA}$ (a) and $a(443)_{QAA}$ (b) for waters of cSPG during the period of July 2002 to July 2020.

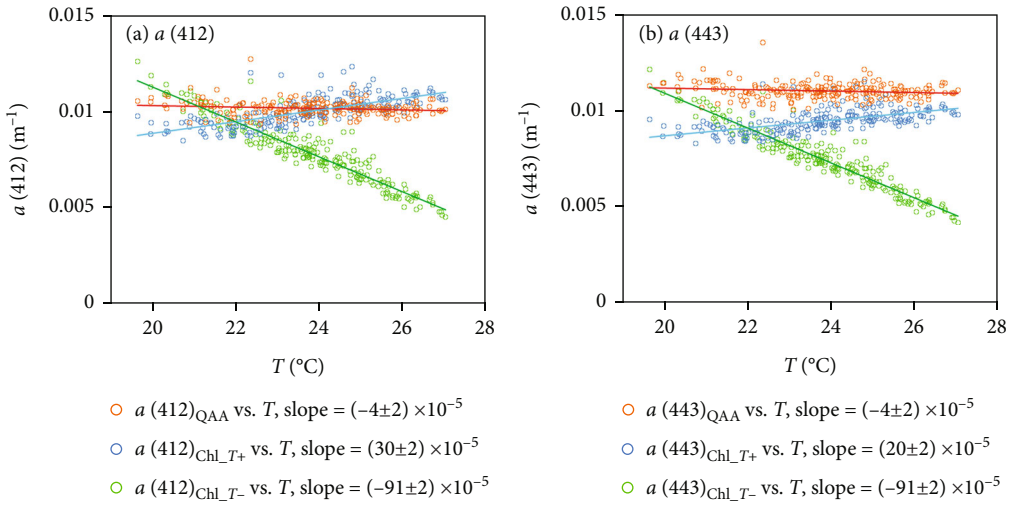

Figure 5: Relationships between T and $a(412)$ (a) and $a(443)$ (b) for waters of cSPG during December–February. The orange, blue, and green circles represent the results of $a(\lambda)_{QAA}$ versus T, $a(\lambda)_{Chl\_T+}$ versus T, and $a(\lambda)_{Chl\_T-}$ versus T, respectively.

Table 1: Linear slope between Chl/a_{ph}/a/a_{fw}/a_{sw} and T.

Location	Property	Number of valid data	Slope^{+} (×10^{-4})	Slope of a_{fw} or a_{sw} (×10^{-4} m^{-1}°C^{-1})				
				B1994^{fw}	T1996^{fw,sw}	P1997^{sw}	S2006^{fw}	R2014^{fw}
HOT*	Chl	81	8 ± 41	\	\	\	\	\
	a_{ph}(410)	34	−0.1 ± 1.7	\	\	\	\	\
	a_{ph}(440)	34	−1.2 ± 3.1	\	\	\	\	\
cSPG**	Chl	216	0.1 ± 0.8	\	\	\	\	\
	$a(412)_{QAA}$	216	−0.4 ± 0.2	13	−9.1 ± 0.6	3 ± 3	0 ± 1	0.04 ± 0.4
	$a(443)_{QAA}$	216	−0.4 ± 0.2	14	−9.1 ± 0.6	2 ± 2	0 ± 0	0.05 ± 0.3

*For data from field measurements in summer months; **for data from MODIS in summer months. $^{+}$The units of slope for Chl versus T and a (or a_{ph} or a_{fw} or a_{sw}) versus T are mg m^{-3}°C^{-1} and m^{-1}°C^{-1}, respectively. B1994, T1996, P1997, S2006, and R2014 represent the T-dependent slope reported in Buiteveld et al. [35], Trabjerg and Hojerslev [7], Pegau et al. [8], Sullivan et al. [9], and Röttgers et al. [10], respectively, where superscripts "fw" and "sw" represent fresh water and salt water.

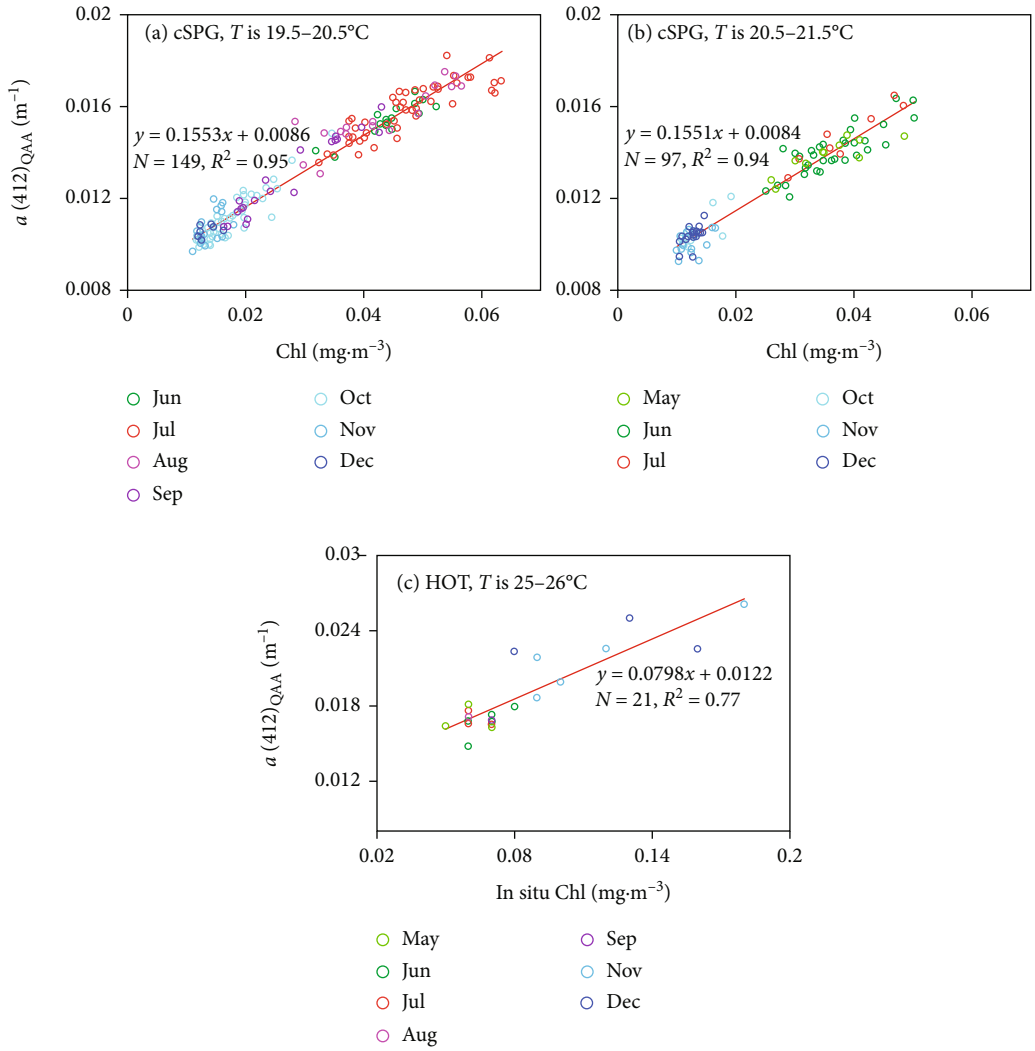

FIGURE 6: Relationships between MODIS Chl and $a(412)_{QAA}$ for T in a range of 19.5–20.5°C (a) and 20.5–21.5°C (b) at cSPG. Also shown is the relationship between *in situ* Chl and $a(412)_{QAA}$ for T in a range of 25–26°C at HOT, where the temperature is in general higher than that at cSPG (see Figure 2).

[7] (represented as $a(\lambda)_{Chl\_T-}$), while the increase of $a(412)$ could be ~26% following Pegau et al. [8] (represented as $a(\lambda)_{Chl\_T+}$).

Can the stable $a(412)_{QAA}$ and $a(443)_{QAA}$ vs. T imply negligible impact of T on $a_{sw}(\lambda)$, at least for T in a range of ~19–27 °C? In general, as shown by Equation (6), $a(\lambda)$ is a sum of $a_{sw}(\lambda)$ and $a_{pg}(\lambda)$ (i.e., $a_{ph} + a_{dg}$). Thus, a stable $a(\lambda)_{QAA}$ could be a result of an increasing $a_{sw}(\lambda)$ with T which is compensated by a decreasing $a_{pg}(\lambda)$, or a decreasing $a_{sw}(\lambda)$ with T is compensated by an increasing $a_{pg}(\lambda)$. This begs the question on how $a_{pg}(\lambda)$ varies in these waters during the summer months.

We first examined the relationship between $a(\lambda)_{QAA}$ and Chl for a given T, i.e., "fixed" $a_{sw}(\lambda)$. As shown in Figures 6(a) and 6(b), for fixed T (T is in a range of 19.5–20.5 °C and 20.5–21.5 °C, respectively), it is found that $a(\lambda)_{QAA}$ highly covary with Chl ($R^2 > 0.94$) at cSPG. This is consistent with that found at HOT (see Figure 6(c)), where for T in a narrow range of 25–26 °C (note that temperature at HOT is always higher than temperature at cSPG), $a(412)_{QAA}$ covaries highly ($R^2 = 0.77$) with *in situ* measured Chl, with a reduced R^2 value due to uncertainties associated with field-measured Chl. These results suggested that indeed Chl is the main driver of the variation of $a(\lambda)_{QAA}$ for such oligotrophic waters. In consequence, during the summer months, the observed constancy of Chl as a function of T (see Figures 2(b) and 2(d)) indicates that $a_{pg}(\lambda)$ also remains stable during this period and over this T range. This is further verified with the time series at HOT (see Figure 7), where field-measured $a_{ph}(410)$ and $a_{ph}(440)$ for the summer months are quite stable (the slope in linear regression between $a_{ph}(410)$ and $a_{ph}(440)$ and T is -1×10^{-5} m^{-1} $°C^{-1}$ and -1×10^{-4} m^{-1} $°C^{-1}$, respectively). These analyses, from both field measurements and satellite observations, suggest that

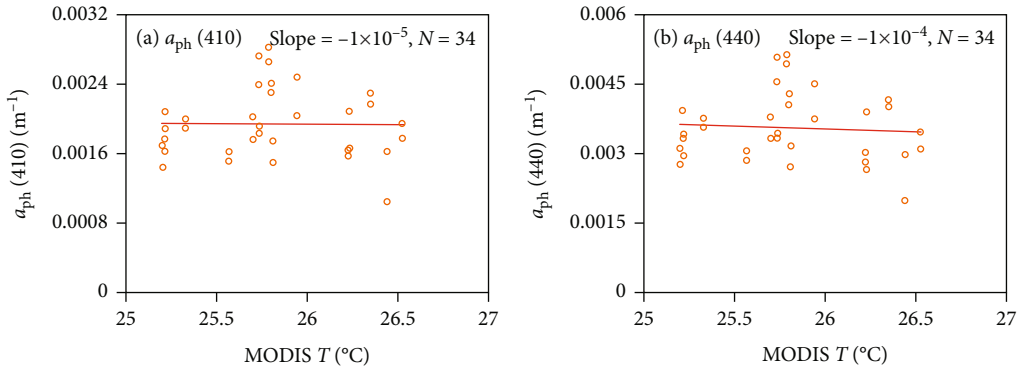

FIGURE 7: Relationship between T and field measured $a_{ph}(410)$ (a) and $a_{ph}(440)$ (b) at HOT for months of July–September in the period of 2006–2013.

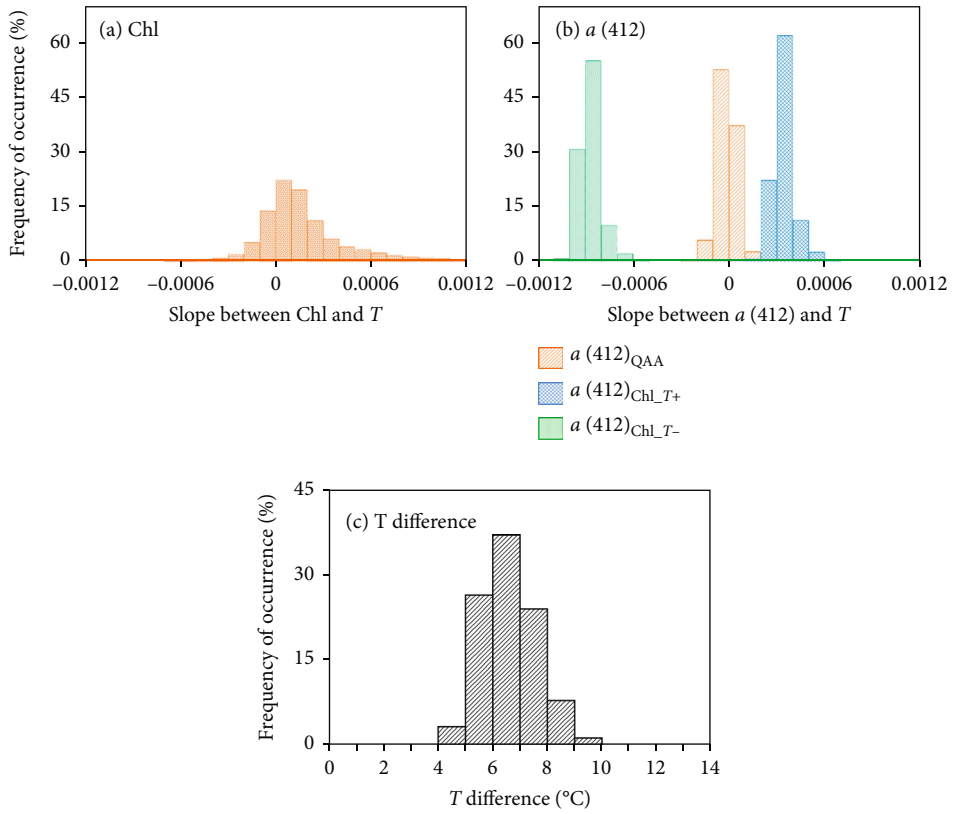

FIGURE 8: The occurrence frequency of slope between T and Chl (a), slope between T and a(412) (b), and T difference (c) in December–February for the entire SPG.

the only viable explanation for a stable $a(412)_{QAA}$ and $a(443)_{QAA}$ over a T range of ~19–27 °C is that values of $a_{sw}(\lambda)$ during summer months are constant (displaying an insignificant negative trend as a function of T).

4.3. Characteristics of $a(412)_{QAA}$, $a(443)_{QAA}$, and T Time Series at SPG. We further extended the above analyses to the entire SPG, which is the regression between Chl or $a(\lambda)$ and T at each pixel in the SPG. The resulted occurrence frequency of these slopes is presented in Figure 8. Since the distribution of slope between $a(443)_{QAA}$ and T derived from each pixel is almost the same as that between $a(412)_{QAA}$ and T, we only present the results of $a(412)_{QAA}$ and Chl. For these summer months, the slope of Chl versus T falls primarily (>91%) in the range of -0.0003 to +0.0006 mg m^{-3} °C^{-1} and ~73% in the range of ±0.0002 mg m^{-3} °C^{-1} (see Figure 8(a)), which translates into the slope between $a_{pg}(\lambda)$ and T being in the order of 10^{-5} m^{-1} °C^{-1} when $a_{pg}(\lambda)$ is derived from Equations (7)–(10). The slope between $a(412)_{QAA}$ and T is generally in the range of -0.0002 to +0.0001 m^{-1} °C^{-1} with ~93% in the order of 10^{-5} m^{-1} °C^{-1} (see Figure 8(b)). This slope, effectively flat, is significantly

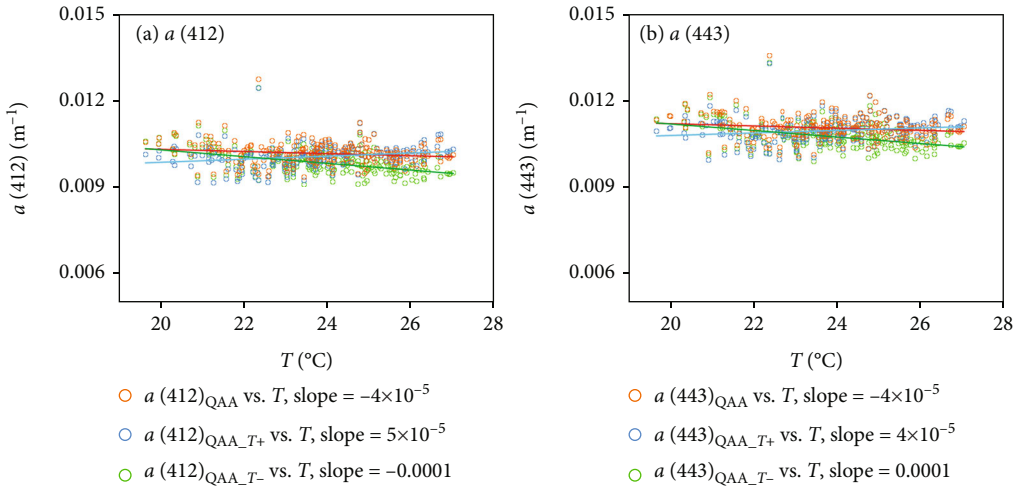

FIGURE 9: Relationships between T and $a(412)_{QAA}$ (a) and $a(443)_{QAA}$ (b) for waters of cSPG during December–February under different Y values. The orange, blue, and green circles represent the results of $a(\lambda)_{QAA}$ of Y not varying with T, Y increases with T, and Y decreases with T.

different from the -0.0009 m^{-1} $°C^{-1}$ reported in Trabjerg and Hojerslev [7] and the 0.0003 m^{-1} $°C^{-1}$ reported in Pegau et al. [8] for $a_{sw}(412)$. Note that the T difference (i.e., the difference of maximum and minimum of T for each pixel) for these months is in the range of 3.9–11.9 °C, with 95% of T difference as 5–9 °C (see Figure 8(c)), which are sufficient to cause detectable variations in a_{sw} in the blue wavelengths based on Trabjerg and Hojerslev [7] and Pegau et al. [8]. Our results, obtained from measurements of natural oceanic waters, are similar to those recently reported in Sullivan et al. [9] and Röttgers et al. [10] (see Table 1), but the latter were from laboratory measurements and for a_{fw}. With regard the challenges of taking precise measurements of a_{fw} or a_{sw} in a laboratory setting [5], these evaluations highlight the value of long-term ocean color satellite measurements in the oligotrophic ocean.

5. Discussion

5.1. Impact of Y on the Temporal Variation of $a(412)_{QAA}$ and $a(443)_{QAA}$. Except for the measurement uncertainties associated with $R_{rs}(\lambda)$, there are two sources of uncertainties for the analytical derivation of $a(412)_{QAA}$ and $a(443)_{QAA}$ via QAA. The first is the model (Equation (1)) to link R_{rs} with a and b_b, while the second is the determination of a Y value (Equation (2)). For uncertainty source 1, there are many models developed in the past [36, 37]. While a different model will result in slightly different retrievals of $a(\lambda)_{QAA}$ [38], here, the focus is on the temporal variation of $a(\lambda)$, not the exact value of $a(\lambda)$; thus, we do not expect that this choice of model for R_{rs} will bring any significant impact on the temporal trend of $a(\lambda)$ as long as it is the same model used for all data. In particular, we focused on a temporal range of summertime when there are almost no visible changes of Chl (see Figure 2).

For uncertainty source 2, a spectral power value (Y) is required (Equation (2)) to calculate $b_{bp}(\lambda)$ from one wavelength to other wavelengths. Historically, researchers set Y value as 2.0 for open-ocean waters [20, 39]. However, it is not known if a temperature-dependent Y will change the patterns. We thus carried out the following numerical experiments to evaluate the potential impact of temperature-dependent Y on $a(412)_{QAA}$ and $a(443)_{QAA}$. For such a sensitivity analysis, we assumed that there could be a decrease or an increase trend of Y for the increase of T, which are expressed as

$$Y_{T+} = 1.5 + 0.1 \times (T - T_r),$$
$$Y_{T-} = 2.0 - 0.1 \times (T - T_r). \quad (11)$$

Here, T_r is a reference temperature which is set as 20 °C; thus, Y is in a range of 1.5–2.5 for T in a range of 20–30 °C under the Y_{T+} scheme, and 2.0–1.0 under Y_{T-} scheme for the same T range. The resulted $a(\lambda)$ via QAA are represented as $a(412)_{QAA\_T+}$ and $a(443)_{QAA\_T-}$ accordingly.

Following the approach used to analyze the trend of $a(\lambda)_{QAA}$ versus T in December–February, the trends of $a(\lambda)_{QAA\_T+}$ and $a(\lambda)_{QAA\_T-}$ versus T are shown in Figure 9. It is found that for these summer months, the slopes between $a(412)_{QAA\_T+}$ and $a(412)_{QAA\_T-}$ and T are still nearly flat (the slope of $a(412)_{QAA\_T+}$ and $a(412)_{QAA\_T-}$ is 4×10^{-5} m^{-1} $°C^{-1}$ and -0.0001 m^{-1} $°C^{-1}$, respectively). In addition, the slopes between $a(443)_{QAA\_T+}$ and $a(443)_{QAA\_T-}$ and T are almost the same with those between $a(412)_{QAA\_T+}$ and $a(412)_{QAA\_T-}$ and T. Thus, for T in a range of 19.6–27 °C, although values of Y vary over a relatively wide range (Y_{T+} is ~1.5–2.2 and Y_{T-} is 2.0–1.3), they have a small influence on the relationship between $a(412)$ and $a(443)$ and T. This is because in these oligotrophic waters, $b_{sw}(412)$ contributes over 50% of $b_b(412)$; thus, a change of Y has limited impact on the derived $a(412)$ for such waters [36]. Further, note that Y changes from 1.5 to 2.5 corresponding to changes in particle-size-class parameter from 4.5 to 5.5 (i.e., significantly more tiny particles) following Kostadinov et al. [40], a variation highly unlikely, especially under a situation where there are no obvious changes of chlorophyll concentration. Thus,

these analyses indicate that the temporal trend between $a(412)$ and $a(443)$ and T obtained from MODIS for the summer months are highly reliable.

5.2. In Principle, What Is Likely the Trend between $a_{fw}(\lambda)$ or $a_{sw}(\lambda)$ and Temperature in the Natural Environment? The discrepancies on the T trends of a_{fw} or a_{sw} in the blue wavelengths reported in the literature [7–10, 35] beg the question of how a_{fw} or a_{sw} should change with T in the natural environment. We know that water has three phases of states: solid (ice), liquid, and gas (water vapor). Although the absorption coefficient of pure ice (a_{w-ice}) is still under debate, it appears that a_{w-ice} is significantly higher than a_{fw} [5, 41, 42], and a_{fw} are significantly higher than that of water vapor. If a_{fw} increases with T, values of a_{fw} will be very high when water is approaching the boiling point. Since the absorption coefficient of water vapor is significantly lower, there must be an abrupt and significant drop of the absorption coefficient when water changes from liquid to water vapor. At the other end, if a_{fw} increases with T, values of a_{fw} will be very low when water is approaching ice; thus, there must be an abrupt and significant increase of the absorption coefficient when liquid water turns to ice water. In short, there will be no continuity of the absorption coefficient when water changes from ice to liquid to gas, if a_{fw} increases with T.

The above considerations support a trend that a_{sw} decreases with T [7], which is also supported by the slightly negative slopes between $a(412)$ and $a(443)$ and T found in this study (see Figures 5 and 8). This is consistent with the nature of water molecules that when T increases, the volume of water molecules expands, thus fewer number of water molecules per unit volume, although this change in volume could be very small, especially for T in the common range of the natural environment. On the other hand, a slope of -0.0009 m^{-1} $^{\circ}C^{-1}$ reported in Trabjerg and Hojerslev [7] appears to be too steep, as $a_{fw}(412)$ will become negative when T simply increases from 20 °C to 23 °C based on the latest $a_{fw}(\lambda)$ values presented in Mason et al. [5].

6. Impact of Salinity on the Absorption Coefficient of Pure Water

The $a_{sw}(\lambda)$ derived by Lee et al. [6] are considerably higher (higher by a factor of 2) than the $a_{fw}(\lambda)$ values recently reported in Mason et al. [5] for λ in the range of 350–420 nm but a bit lower than that of Mason et al. [5] for $\lambda > 430$ nm. This difference is not surprising because the waters considered in Lee et al. [6] are oceanic waters where the average salinity is about 35 PSU [43], with an average T similar to that in Mason et al. [5]. Therefore, the difference between the $a_{sw}(\lambda)$ values in Lee et al. [6] (a_{sw_L15}) and the $a_{fw}(\lambda)$ values in Mason et al. [5] (a_{fw_M16}) suggests an impact of salinity on the absorption coefficient of pure water. Assuming this impact is linearly related to salinity [10], then a slope of salinity can be calculated from the two independent determinations (represented as Ψ_{S-LM})

$$\Psi_{S\text{-}LM} = \frac{a_{sw_{L15}} - a_{fw_{M16}}}{35.0}. \quad (12)$$

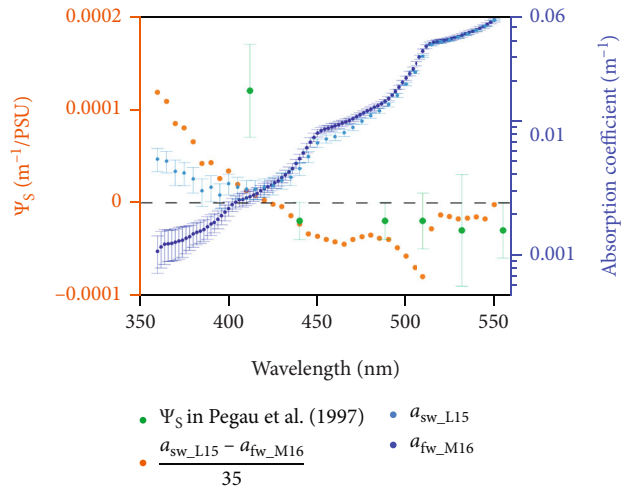

FIGURE 10: Salinity slope (Ψ_s, left Y axis) of $a_{sw}(\lambda)$ reported in Pegau et al. [8] (green dots) and the values (orange dots) calculated based on the difference between $a_{sw}(\lambda)$ in Lee et al. [6] (a_{sw_L15}) and $a_{fw}(\lambda)$ in Mason et al. [5] (a_{fw_M16}). Right Y axis for absorption coefficient.

When Ψ_{s-LM} values are compared with the salinity slopes reported in Pegau et al. [8] (represented as Ψ_{s-P}; see Figure 10), we find good agreement with Ψ_{s-P} for λ in the range of ~400–550 nm. In particular, these determinations show positive salinity slope at 410 nm and negative salinity slopes for λ longer than ~430 nm, remarkable agreements from these independent determinations. But the Ψ_{s-P} value is much higher than Ψ_{s-LM} at 410 nm, which could be due to CDOM contamination in the artificial seawater solutions, or an over correction for CDOM contribution in the derivation of $a_{sw}(\lambda)$ in Lee et al. [6], which deserve further studies from a well-controlled experiment. On the other hand, these findings are different from that of Sullivan et al. [9] and Röttgers et al. [10], where no detectable salt effect on $a_{fw}(\lambda)$ was found. In view of the significant differences in $a_{fw}(\lambda)$ in the blue wavelengths reported between Pope and Fry [4] and Mason et al. [5], and that Röttgers et al. [10] indicated that the salinity slopes in their study are unreliable for wavelengths < 500 nm, it highlights the challenges to obtain accurate measurements of such properties in laboratory settings.

7. Conclusions

Based on field measured Chl, a_{ph}, T and ~18 years (from 2002 to 2020) of MODIS ocean color measurements in the oligotrophic oceans, we analyzed the relationships between $a(412)$ and $a(443)$ and T. We found that, for the summer months of the southern hemisphere (December–February) in the center of the South Pacific Gyre (SPG) where T varied from ~19 to 27 °C, the slope between $a(412)$ and $a(443)$ and T is nearly 0 (in the order of 10^{-5}, slightly negative), which indicates stable values of $a_{sw}(\lambda)$ within this temperature range. Such a stable pattern is further confirmed when analyzing the entire SPG. Our results are similar to those reported in Sullivan et al. [9] and Röttgers et al. [10] regarding the impact of T on water's absorption coefficient, but the

latter were obtained from laboratory measurements of prepared "pure" water. Further, the slight negative trend with T for $a(412)$ and $a(443)$ is consistent with the reduced number of water molecules per volume when T increases in a common natural environment, although such a change is very small. Thus, in principle, $a_{sw}(\lambda)$ in the blue wavelengths are decreasing with an increase of T, although the actual effect could be negligible for the purpose of retrieving ocean color products from remote-sensing observations.

Separately, based on previously reported $a_{sw}(\lambda)$ [6] and $a_{fw}(\lambda)$ [5], we calculated the salinity slope for λ in the range of ~350–550 nm, with results in good agreement with that of Pegau et al. [8]. These results, from three independent determinations, do suggest an impact of salinity on $a_{fw}(\lambda)$. As demonstrated in Yu et al. [44], for processing ocean color measurements in the oceanic waters, it is better to adopt $a_{sw}(\lambda)$ rather than $a_{fw}(\lambda)$; otherwise, more uncertainties will be introduced in the retrieved $a_{ph}(\lambda)$.

Note that the selection of the wavelengths in this study is constrained by the band configuration of the satellite sensor. After we obtain long-term hyperspectral R_{rs} in the oligotrophic ocean, the above analysis can be extended to evaluate the effect of T on hyperspectral $a_{sw}(\lambda)$. Separately, compared to the high demand of caution in sample preparations and sensors' calibrations in laboratory measurements of such properties, the long-term satellite data offer a unique and reliable data source to evaluate the impact of temperature on the "pure"seawater absorption coefficient, but the calibration of an ocean color satellite sensor does require a significant effort from the community.

Data Availability

The satellite and *in situ* data used to support the findings of this study are publicly available. MODIS-Aqua data can be downloaded from the NASA OBPG website (http://oceancolor.gsfc.nasa.gov/), while field measurements of HOT can be found online at https://hahana.soest.hawaii.edu/hot/.

Conflicts of Interest

The authors declare that there are no conflicts of interest regarding the publication of this article.

Authors' Contributions

GW processed and analyzed the data and drafted the manuscript, ZL conceptualized the study and finalized the manuscript, XW helped with the MODIS data processing, XY and SS helped with the data analysis and manuscript preparation, and RL provided *in situ* data and revised the manuscript.

Acknowledgments

Financial support provided by the National Natural Science Foundation of China (#41890803, #41941008, and #41830102), the Joint Polar Satellite System (JPSS) funding for the NOAA ocean color calibration and validation (Cal/Val) project (SA18-UMB01), and the University of Massachusetts Boston is greatly appreciated. We thank NASA OBPG for processing and providing global MODIS ocean color data and the Hawaii Ocean Time-series HOT-DOGS application (University of Hawai'i at Mānoa, National Science Foundation Award #1756517) for data collection and sharing.

References

[1] R. W. Preisendorfer, *Hydrologic optics*, vol. 6, U.S. Dept. of Commerce, National Oceanic and Atmospheric Administration, Environmental Research Laboratories, Pacific Marine Environmental Laboratory, Honolulu, 1976.

[2] H. R. Gordon and A. Y. Morel, "Remote assessment of ocean color for interpretation of satellite visible imagery: a review," in *Lecture notes on coastal and estuarine studies*, R. T. Barber, C. N. K. Mooers, M. J. Bowman, and B. Zeitzschel, Eds., Springer-Verlag, New York, 1983.

[3] M. P. Fewell and A. von Trojan, "Absorption of light by water in the region of high transparency: recommended values for photon-transport calculations," *Applied Optics*, vol. 58, no. 9, pp. 2408–2421, 2019.

[4] R. M. Pope and E. S. Fry, "Absorption spectrum (380-700 nm) of pure water II integrating cavity measurements," *Applied Optics*, vol. 36, no. 33, pp. 8710–8723, 1997.

[5] J. D. Mason, M. T. Cone, and E. S. Fry, "Ultraviolet (250-550 nm) absorption spectrum of pure water," *Applied Optics*, vol. 55, no. 25, pp. 7163–7172, 2016.

[6] Z. Lee, J. Wei, K. Voss, M. Lewis, A. Bricaud, and Y. Huot, "Hyperspectral absorption coefficient of "pure" seawater in the range of 350-550 nm inverted from remote sensing reflectance," *Applied Optics*, vol. 54, no. 3, pp. 546–558, 2015.

[7] I. Trabjerg and N. K. Hojerslev, "Temperature influence on light absorption by fresh water and seawater in the visible and near-infrared spectrum," *Applied Optics*, vol. 35, no. 15, pp. 2653–2658, 1996.

[8] W. S. Pegau, D. Gray, and J. R. V. Zaneveld, "Absorption and attenuation of visible and near-infrared light in water: dependence on temperature and salinity," *Applied Optics*, vol. 36, no. 24, pp. 6035–6046, 1997.

[9] J. M. Sullivan, M. S. Twardowski, J. R. V. Zaneveld et al., "Hyperspectral temperature and salt dependencies of absorption by water and heavy water in the 400-750 nm spectral range," *Applied Optics*, vol. 45, no. 21, pp. 5294–5309, 2006.

[10] R. Röttgers, D. McKee, and C. Utschig, "Temperature and salinity correction coefficients for light absorption by water in the visible to infrared spectral region," *Optics Express*, vol. 22, no. 21, pp. 25093–25108, 2014.

[11] R. M. Letelier, A. E. White, R. R. Bidigare, B. Barone, M. J. Church, and D. M. Karl, "Light absorption by phytoplankton in the North Pacific Subtropical Gyre," *Limnology and Oceanography*, vol. 62, no. 4, pp. 1526–1540, 2017.

[12] A. Morel, B. Gentili, H. Claustre et al., "Optical properties of the "clearest" natural waters," *Limnology and Oceanography*, vol. 52, no. 1, pp. 217–229, 2007.

[13] C. R. McClain, S. R. Signorini, and J. R. Christian, "Subtropical gyre variability observed by ocean-color satellites," *Deep-Sea Research Part Ii-Topical Studies in Oceanography*, vol. 51, no. 1-3, pp. 281–301, 2004.

[14] J. J. Polovina, E. A. Howell, and M. Abecassis, "Ocean's least productive waters are expanding," *Geophysical Research Letters*, vol. 35, no. 3, 2008.

[15] E. Leymarie, D. Doxaran, and M. Babin, "Uncertainties associated to measurements of inherent optical properties in natural waters," *Applied Optics*, vol. 49, no. 28, pp. 5415–5436, 2010.

[16] N. D. Stockley, R. Rottgers, D. Mckee, I. Lefering, J. M. Sullivan, and M. S. Twardowski, "Assessing uncertainties in scattering correction algorithms for reflective tube absorption measurements made with a WET labs ac-9," *Optics Express*, vol. 25, no. 24, pp. A1139–A1153, 2017.

[17] Z. Lee, C. Hu, S. Shang et al., "Penetration of UV-visible solar radiation in the global oceans: insights from ocean color remote sensing," *Journal of Geophysical Research-Oceans*, vol. 118, no. 9, pp. 4241–4255, 2013.

[18] H. R. Gordon and W. R. McCluney, "Estimation of the depth of sunlight penetration in the sea for remote sensing," *Applied Optics*, vol. 14, no. 2, pp. 413–416, 1975.

[19] IOCCG, "Remote sensing of inherent optical properties: fundamentals, tests of algorithms, and applications," in *Reports of the International Ocean-Colour Coordinating Group, No. 5*, Z.-P. Lee, Ed., IOCCG, Dartmouth, Canada, 2006.

[20] Z. Lee, K. L. Carder, and R. A. Arnone, "Deriving inherent optical properties from water color: a multiband quasi-analytical algorithm for optically deep waters," *Applied Optics*, vol. 41, no. 27, pp. 5755–5772, 2002.

[21] J. R. V. Zaneveld, "A theoretical derivation of the dependence of the remotely-sensed reflectance of the ocean on the inherent optical-properties," *Journal of Geophysical Research-Oceans*, vol. 100, no. C7, pp. 13135–13142, 1995.

[22] X. D. Zhang, L. B. Hu, and M. X. He, "Scattering by pure seawater: effect of salinity," *Optics Express*, vol. 17, no. 7, pp. 5698–5710, 2009.

[23] C. M. Hu, Z. Lee, and B. Franz, "Chlorophyllaalgorithms for oligotrophic oceans: a novel approach based on three-band reflectance difference," *Journal of Geophysical Research-Oceans*, vol. 117, no. C1, article C01011, 2012.

[24] A. Bricaud, M. Babin, A. Morel, and H. Claustre, "Variability in the chlorophyll-specific absorption-coefficients of natural phytoplankton - analysis and parameterization," *Journal of Geophysical Research-Oceans*, vol. 100, no. C7, pp. 13321–13332, 1995.

[25] A. Bricaud, A. Morel, M. Babin, K. Allali, and H. Claustre, "Variations of light absorption by suspended particles with chlorophyll a concentration in oceanic (case 1) waters: analysis and implications for bio-optical models," *Journal of Geophysical Research-Oceans*, vol. 103, no. C13, pp. 31033–31044, 1998.

[26] S. Maritorena, D. A. Siegel, and A. R. Peterson, "Optimization of a semianalytical ocean color model for global-scale applications," *Applied Optics*, vol. 41, no. 15, pp. 2705–2714, 2002.

[27] A. Morel, "Optical modeling of the upper ocean in relation to its biogenous matter content (case I waters)," *Journal of Geophysical Research-Oceans*, vol. 93, no. C9, pp. 10749–10768, 1988.

[28] A. Morel, Y. Huot, B. Gentili, P. J. Werdell, S. B. Hooker, and B. A. Franz, "Examining the consistency of products derived from various ocean color sensors in open ocean (case 1) waters in the perspective of a multi-sensor approach," *Remote Sensing of Environment*, vol. 111, no. 1, pp. 69–88, 2007.

[29] A. Morel and B. Gentili, "A simple band ratio technique to quantify the colored dissolved and detrital organic material from ocean color remotely sensed data," *Remote Sensing of Environment*, vol. 113, no. 5, pp. 998–1011, 2009.

[30] A. Morel, H. Claustre, and B. Gentili, "The most oligotrophic subtropical zones of the global ocean: similarities and differences in terms of chlorophyll and yellow substance," *Biogeosciences*, vol. 7, no. 10, pp. 3139–3151, 2010.

[31] A. Bricaud, M. Babin, H. Claustre, J. Ras, and F. Tieche, "Light absorption properties and absorption budget of Southeast Pacific waters," *Journal of Geophysical Research-Oceans*, vol. 115, no. C8, article C08009, 2010.

[32] R. M. Letelier, R. R. Bidigare, D. V. Hebel, M. Ondrusek, C. D. Winn, and D. M. Karl, "Temporal variability of phytoplankton community structure-based on pigment analysis," *Limnology and Oceanography*, vol. 38, no. 7, pp. 1420–1437, 1993.

[33] C. D. Winn, L. Campbell, J. R. Christian et al., "Seasonal variability in the phytoplankton community of the North Pacific Subtropical Gyre," *Global Biogeochemical Cycles*, vol. 9, no. 4, pp. 605–620, 1995.

[34] M. J. Behrenfeld, R. T. O'Malley, D. A. Siegel et al., "Climate-driven trends in contemporary ocean productivity," *Nature*, vol. 444, no. 7120, pp. 752–755, 2006.

[35] H. Buiteveld, J. H. M. Hakvoort, and M. Donze, "The optical properties of pure water," *Ocean Optics*, vol. XII, 1994.

[36] Z. Lee, R. Arnone, C. Hu, P. J. Werdell, and B. Lubac, "Uncertainties of optical parameters and their propagations in an analytical ocean color inversion algorithm," *Applied Optics*, vol. 49, no. 3, pp. 369–381, 2010.

[37] Y. J. Park and K. Ruddick, "Model of remote-sensing reflectance including bidirectional effects for case 1 and case 2 waters," *Applied Optics*, vol. 44, no. 7, pp. 1236–1249, 2005.

[38] W. Zhou, J. Lin, and R. Ma, "Effects of forward models on the semi-analytical retrieval of inherent optical properties from remote sensing reflectance," *Applied Optics*, vol. 58, no. 13, pp. 3509–3527, 2019.

[39] S. A. Garver and D. A. Siegel, "Inherent optical property inversion of ocean color spectra and its biogeochemical interpretation. 1. Time series from the Sargasso Sea," *Journal of Geophysical Research-Oceans*, vol. 102, no. C8, pp. 18607–18625, 1997.

[40] T. S. Kostadinov, D. A. Siegel, and S. Maritorena, "Retrieval of the particle size distribution from satellite ocean color observations," *Journal of Geophysical Research-Oceans*, vol. 114, no. C9, article C09015, 2009.

[41] S. G. Warren, R. E. Brandt, and T. C. Grenfell, "Visible and near-ultraviolet absorption spectrum of ice from transmission of solar radiation into snow," *Applied Optics*, vol. 45, no. 21, pp. 5320–5334, 2006.

[42] D. K. Perovich and J. W. Govoni, "Absorption-coefficients of ice from 250 to 400 nm," *Geophysical Research Letters*, vol. 18, no. 7, pp. 1233–1235, 1991.

[43] H. Claustre, A. Sciandra, and D. Vaulot, "Introduction to the special section bio-optical and biogeochemical conditions in the South East Pacific in late 2004: the BIOSOPE program," *Biogeosciences*, vol. 5, no. 3, pp. 679–691, 2008.

[44] X. L. Yu, Z. Lee, J. Wei, and S. Shang, "Impacts of pure seawater absorption coefficient on remotely sensed inherent optical properties in oligotrophic waters," *Optics Express*, vol. 27, no. 24, pp. 34974–34984, 2019.